


Nonlinear Quantum Electrodynamics in Dirac Materials

Aydın Cem Keser^{1,2}, Yuli Lyanda-Geller,³ and Oleg P. Sushkov^{1,2}

¹*School of Physics, University of New South Wales, Sydney, New South Wales 2052, Australia*

²*Australian Research Council Centre of Excellence in Low-Energy Electronics Technologies, University of New South Wales, Sydney, New South Wales 2052, Australia*

³*Department of Physics and Astronomy, Purdue University, West Lafayette, Indiana 47907, USA*

 (Received 29 January 2021; revised 28 October 2021; accepted 13 January 2022; published 11 February 2022)

Classical electromagnetism is linear. However, fields can polarize the vacuum Dirac sea, causing quantum nonlinear electromagnetic phenomena, e.g., scattering and splitting of photons, that occur only in very strong fields found in neutron stars or heavy ion colliders. We show that strong nonlinearity arises in Dirac materials at much lower fields ~ 1 T, allowing us to explore the nonperturbative, extremely high field limit of quantum electrodynamics in solids. We explain recent experiments in a unified framework and predict a new class of nonlinear magnetoelectric effects, including a magnetic enhancement of dielectric constant of insulators and a strong electric modulation of magnetization. We propose experiments and discuss the applications in novel materials.

DOI: [10.1103/PhysRevLett.128.066402](https://doi.org/10.1103/PhysRevLett.128.066402)

Classical electromagnetism is linear and hence supports the principle of superposition. It has been pointed out by Heisenberg and Euler in 1936 that, due to quantum mechanical effects and the presence of the Dirac sea, linearity ceases to hold in strong fields [1]. Quantum electrodynamics (QED) is therefore nonlinear as the electromagnetic field polarizes the Dirac sea as though it is a material medium. This effect becomes significant at electric and magnetic fields $E_* \simeq 1.3 \times 10^{16}$ V/cm and $B_* \simeq 4.4 \times 10^9$ T, at which the Zeeman splitting and electric potential over the Compton wavelength become comparable to the electron rest energy. These are the so-called Schwinger critical values [2] and they are enormous on the laboratory scale. Such fields exist only in exotic environments, e.g., neutron stars [3] and heavy ion colliders [4]. Nevertheless, some low-order nonlinear QED effects, such as scattering or splitting of photons, have been observed in the laboratory [5,6], and probing strong field effects is an active area of research [7].

Dirac materials have been known for decades [8–10]. Nevertheless, their recently understood topological properties and surface excitations have led to a surge of interest [11–16]. The nonlinear electromagnetic response of Dirac materials have been studied [16–23] due to their transport properties (e.g., rectification) and possible applications in photovoltaics. In this Letter, rather than transport, we study dielectric and magnetization response of the three-dimensional (3D) Dirac insulators and semimetals due to the Dirac vacuum, i.e., filled valence band. We include nonlinear contributions to all orders by nonperturbatively analyzing the Heisenberg-Euler action [1,24–27], going both beyond known results of QED and the general framework in condensed matter physics [28]. In known

Dirac materials, we find the typical values of Schwinger fields, $E_* \sim 10^5$ V/cm and $B_* \sim 1$ T, that are easily accessible, providing a platform to explore the strong field regime of QED and to observe quantum nonlinear electromagnetic effects in the laboratory.

The nonlinear effects contribute to the experimentally observed high field magnetization in the recent work on the Weyl semimetal TaAs [31] and the Dirac semimetal Bi [32], but the importance of this observation and its origin in the Heisenberg-Euler effect has not been recognized. In the present Letter, we demonstrate this connection and show that the data [31,32] agree with our predictions. More importantly, we predict a new class of magnetoelectric effects. The most significant is the magnetic field tunable, very large enhancement of the dielectric constant, reaching up to $\delta\epsilon_r \sim 10$ per every 1 T of the applied magnetic field. We also predict an electric field modulated magnetization. Both these effects are highly anisotropic, that is, they depend on relative orientation of E and B fields and their crystallographic orientation.

In a material, the classical Lagrangian of the electromagnetic field is [33]

$$L_{\text{cl}} = \frac{1}{8\pi} (\mathbf{E}^T \boldsymbol{\epsilon} \mathbf{E} - \mathbf{B}^T \boldsymbol{\mu}^{-1} \mathbf{B}). \quad (1)$$

One of our principal results is the quantum one-loop, nonlinear, nonperturbative contribution to the Lagrangian

$$\delta L_{\text{HE}} \rightarrow \frac{\Delta}{24\pi^2 \lambda_D^3} [(\mathbf{b} \cdot \mathbf{e})^2 |\mathbf{b}|^{-1} + |\mathbf{b}|^2 \ln |\mathbf{b}|], \quad (2)$$

TABLE I. Comparison of parameters including the band gap (2Δ) [65], effective fine structure constant $\alpha_D = (e^2/\hbar v)$ as the ratio $\alpha_D/\alpha = c/v$, and the Schwinger fields in Eq. (4).

	2Δ (meV)	α_D/α	E_* (V/cm)	B_* (mT)
QED ($\Delta = m_e c^2$)	10^9 [69,70]	1	1.3×10^{16}	4.4×10^{12}
Pb _{0.5} Sn _{0.5} Te	63 [71]	580	2.9×10^4	5.6×10^3
Bi _{0.9} Sb _{0.1}	15.5 [72,73]	188	571	36
TaAs	0	357	0	0

in a strong B and weak E field (see further below and also Sec. S6 of the Supplemental Material [34]). Here, the dimensionless vectors \mathbf{e} and \mathbf{b} depend on the fine structure constant $\alpha_D = e^2/\hbar v$ of the Dirac material,

$$\mathbf{e}(\alpha_D) = \frac{\mathcal{U}\mathbf{E}}{E_*(\alpha_D)}, \quad \mathbf{b}(\alpha_D) = \frac{\mathcal{U}^{-1}\mathbf{B}}{B_*(\alpha_D)}, \quad (3)$$

and the critical ‘‘Schwinger’’ electric $E_*(\alpha_D)$ and magnetic $B_*(\alpha_D)$ fields in the material are defined by

$$E_*^2(\alpha_D) = \frac{v^2}{c^2} B_*^2(\alpha_D) = \frac{\Delta}{\alpha_D \lambda_D^3} = \left(\frac{\Delta^2}{e\hbar v} \right)^2. \quad (4)$$

Equations (2)–(4) account for the anisotropy of real materials [64], for which the velocity tensor is a 3×3 symmetric matrix [10] $\mathcal{V} = v\mathcal{U}$, with $\det(\mathcal{U}) = 1$. The terms $\mathcal{U}\mathbf{E}$ and $\mathcal{U}^{-1}\mathbf{B}$ are linear transformations of \mathbf{E} and \mathbf{B} , respectively (see Supplemental Material Sec. S1 [34]).

We have defined the symbols in Eqs. (3) and (4) according to convention in QED. The ‘‘Dirac wavelength’’ $\lambda_D = (\hbar v/\Delta)$ and the ‘‘Dirac magneton’’ $\mu_D = (e\hbar v^2/2\Delta c)$ replace the Compton wavelength and the Bohr magneton, respectively. When the fields reach the Schwinger scale, Zeeman splitting and the potential difference at λ_D are equal to half of the Dirac band gap,

$$2\mu_D B_* = \lambda_D e E_* = \Delta, \quad (5)$$

and the nonlinearity becomes relevant. In Table I we list material parameters considered in this Letter. For more details, see Sec. S2 and Table S1 of the Supplemental Material [34].

The quantum contribution to the Lagrangian can be viewed as the sum of the infinite chain of one-loop diagrams in Fig. 1 that represent the polarization of the Dirac sea of electrons by external electric and magnetic fields. In this Letter, we consider only nonmagnetic crystals with inversion symmetry [74,75] and assume the static (quasistatic) approximation, $\omega, kv \ll \Delta$, where ω and k are the frequency and the wave number of the external fields. Therefore our diagrams, Fig. 1, have only even numbers of external E and B lines. Besides diagrams in Fig. 1, there are also multiloop diagrams suppressed by a factor of

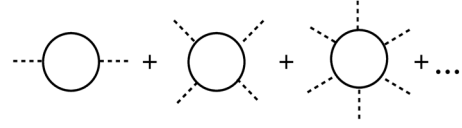


FIG. 1. Diagrammatic representation of the Heisenberg-Euler action $\delta L_1 + \delta L_{\text{HE}}$ [Eqs. (6) and (9)]. The dashed line corresponds to the constant external electromagnetic fields B, E and the solid line is the Green’s function of a Dirac sea electron.

$\alpha_D/\epsilon \sim 0.03$ per each additional loop, where ϵ is the large dielectric constant mainly due to the lattice and intraionic polarization. For the discussion of the suppression of the multiloop diagrams in the context of phenomena considered here, see Sec. S3 in the Supplemental Material [34] and also Refs. [76,77].

In Fig. 1, the first diagram quadratic in external fields is ultraviolet divergent and is equal to [24,65]

$$\delta L_1 = \frac{\Delta}{12\pi^2 \lambda_D^3} \ln\left(\frac{\Lambda}{\Delta}\right) (|\mathbf{e}|^2 - |\mathbf{b}|^2). \quad (6)$$

Here the subscript ‘‘1’’ indicates contribution from the first diagram in Fig. 1 and $\Lambda \sim v(\hbar\pi/a) \sim 1$ eV is the ultraviolet cutoff energy, where a is the lattice spacing. In QED this diagram describes the electric permittivity and magnetic permeability of vacuum, and thus it is included in the definitions of the electric charge and electromagnetic fields. As a result, δL_1 does not appear explicitly in QED. However, for Dirac materials δL_1 is an explicit contribution that has to be added to the classical Lagrangian (1). Indeed, this is the contribution of the Dirac sea (valence band) to the dielectric constant and magnetic susceptibility.

Equating $(E^2 - B^2)/(8\pi) + \delta L_1$ to the classical Lagrangian (1), we find the linear dielectric constant ϵ_D and the linear magnetic susceptibility χ_D ($\boldsymbol{\mu} = \mathbf{1} + 4\pi\boldsymbol{\chi}$),

$$\epsilon_D = \mathbf{1} + \frac{2\alpha_D}{3\pi} \ln\left(\frac{\Lambda}{\Delta}\right) \mathcal{U}^2, \quad \epsilon_D \sim 3, \quad (7)$$

$$\chi_D = -\frac{\alpha_D}{6\pi^2} \frac{v^2}{c^2} \ln\left(\frac{\Lambda}{\Delta}\right) \mathcal{U}^{-2}, \quad \chi_D \sim -10^{-6}, \quad (8)$$

where estimates are given for the diagonalized tensors.

Equations (7) and (8) define the Dirac contributions to the total dielectric and magnetic susceptibilities. The contribution (7) is relatively small compared to the total relative permittivity ϵ in Eq. (1), typically $\epsilon \sim 100$, which is primarily due to the ionic (lattice) and intraionic contributions (see Supplemental Material Table S2 [34]). The magnetic response (8) constitutes a significant part of the diamagnetic susceptibility, which also has contributions from lower bands and core electrons. For bismuth, the Dirac valence band contribution (8) has been previously considered in Ref. [78].

We describe now the nonlinear effects. The diagrams in Fig. 1 beyond the first one ($n \geq 2$) are convergent at arbitrarily large $|\mathbf{e}|$, $|\mathbf{b}|$ [79] and are resummed exactly [80] to yield the one-loop, nonperturbative Heisenberg-Euler action

$$\delta L_{\text{HE}} = \sum_{n=2}^{\infty} \delta L_n \equiv \frac{-\Delta}{8\pi^2 \lambda_D^3} \int_0^{\infty} \frac{d\eta e^{-\eta}}{\eta} \times \left[A_- \cot(\eta A_-) A_+ \cot(\eta A_+) - \frac{1}{\eta^2} + \frac{1}{3} (A_-^2 + A_+^2) \right],$$

$$A_{\mp} = -\frac{i}{2} \left[\sqrt{(\mathbf{b} + i\mathbf{e})^2} \mp \sqrt{(\mathbf{b} - i\mathbf{e})^2} \right], \quad (9)$$

which accounts for crystal anisotropy, cf. Eq. (3), as well as the strong electric and magnetic field behavior. The imaginary part of Eq. (9), obtained via its analytic continuation, captures the dielectric breakdown, which can be avoided in weak electric fields $|\mathbf{e}| < 1$ ($E < E_*$). Then, Eq. (9) can be expanded in powers of \mathbf{e} . However, the magnetic field can be much larger than B_* , leading to the asymptotic expression (2) (see Supplemental Material Sec. S6 [34]). At weak magnetic fields, $|\mathbf{e}|$, $|\mathbf{b}| \ll 1$, Eq. (9) reduces to the second diagram in Fig. 1,

$$\delta L_2 = \frac{\Delta}{360\pi^2 \lambda_D^3} [(|\mathbf{e}|^2 - |\mathbf{b}|^2)^2 + 7(\mathbf{e} \cdot \mathbf{b})^2]. \quad (10)$$

At $E = 0$, the nonlinear magnetic susceptibility is

$$\delta\chi = \frac{\partial^2 \delta L_{\text{HE}}}{\partial \mathbf{B} \partial \mathbf{B}} = \mathcal{U}^{-2} \frac{\alpha_D}{12\pi^2} \frac{v^2}{c^2} F(|\mathbf{b}|);$$

$$F(|\mathbf{b}|) = \frac{2}{5} |\mathbf{b}|^2, \quad |\mathbf{b}| \ll 1,$$

$$F(|\mathbf{b}|) = \ln |\mathbf{b}|, \quad |\mathbf{b}| \gg 1. \quad (11)$$

The dimensionless function $F(|\mathbf{b}|)$ in the full range of magnetic fields obtained by numerical integration of Eq. (9) is shown in Supplemental Material Fig. S2 [34]. Strong and weak field limits of F follow from the actions given by Eqs. (2) and (10), respectively.

The total magnetic susceptibility of the Dirac valence band is the sum of the linear susceptibility, Eq. (8), and the nonlinear contribution $\chi = \chi_D + \delta\chi$. When $|\mathbf{b}| \gg 1$, we have

$$\chi = -\mathcal{U}^{-2} \frac{\alpha_D}{12\pi^2} \frac{v^2}{c^2} \ln \left(\frac{c\Lambda^2}{e|\mathcal{U}^{-1}\mathbf{B}|\hbar v^2} \right). \quad (12)$$

Here χ depends on B but not on Δ and is well defined in the limit $\Delta = 0$, as in the Weyl semimetal TaAs [31].

According to Eqs. (11) and (12), the magnetic susceptibility is nonlinear, i.e., it depends on magnetic field. Remarkably, this Dirac nonlinearity has been recently observed, but its connection to nonlinear electrodynamics

was not identified. Here we show its origin in the Heisenberg-Euler effect. The magnetization of Weyl semimetal TaAs has been measured up to $B = 30$ T, Ref. [31], and magnetization of Dirac semimetal Bi has been measured up to $B = 60$ T, Ref. [32]. In Zhang *et al.* [31], the valence band contribution to magnetization at $\mathbf{E} = 0$ was considered [81], and in the high magnetic field limit, the magnetization quasilinear in the applied B field is investigated. Here we study the universal *nonlinear* susceptibility and eliminate all uncertainties, such as the choice of ultraviolet cutoff Λ , subleading terms, and contributions from other bands or core electrons.

Both TaAs and Bi have nonzero chemical potential and hence have conduction electrons. Therefore, at weak magnetic fields, both compounds show magnetic oscillations. The conduction electrons freeze and the oscillations disappear at $B > 5$ T in Bi [32] and $B > 10$ –13 T in TaAs [31]. In these ranges of B , we can compare the data with our predictions. In Fig. 2(a), the points show magnetic susceptibilities of TaAs (c direction) and Bi (binary and bisectrix directions). The points have significant spread, as they are obtained by numerical differentiation of experimental magnetizations from Refs. [31,32]. To focus on the nonlinearity, we plot $\chi_{\text{ref}} - \chi$, where $\chi_{\text{ref}} = \chi(B = 30)$ T for TaAs and $\chi_{\text{ref}} = \chi(B = 50)$ T for Bi. Solid curves present our theoretical predictions, which are manifestly consistent with the data. For discussion of material specific details, anisotropy, etc., see Supplemental Material Sec. S8 [34]. Interestingly, Bi_{0.9}Sb_{0.1} alloy has the band structure very close to that of Bi, but with no conduction electrons [72,73], and could be an ideal test platform for our theory. The susceptibility of this compound has not been measured yet. Our theoretical prediction is shown by the solid red curve in Fig. 2(a).

We now consider novel magnetoelectric effects. The nonlinear dielectric constant is

$$\delta\epsilon_D = 4\pi \frac{\partial^2 \delta L_{\text{HE}}}{\partial \mathbf{E} \partial \mathbf{E}} = \mathcal{U}^2 \frac{\alpha_D}{3\pi} G_i(|\mathbf{b}|);$$

$$|\mathbf{b}| \ll 1: G_{||}(|\mathbf{b}|) = \frac{1}{3} |\mathbf{b}|^2, \quad G_{\perp}(|\mathbf{b}|) = -\frac{2}{15} |\mathbf{b}|^2,$$

$$|\mathbf{b}| \gg 1: G_{||}(|\mathbf{b}|) = |\mathbf{b}|, \quad G_{\perp}(|\mathbf{b}|) = -\ln(|\mathbf{b}|). \quad (13)$$

Here the index $i = ||, \perp$ shows the relative orientation of \mathbf{e} and \mathbf{b} [82]. Dimensionless functions $G_i(|\mathbf{b}|)$ in the whole range of \mathbf{b} obtained by numerical integration of (9) are plotted in Supplemental Material Fig. S2 [34]. Its strong and weak field limits define actions given by Eqs. (2) and (10), respectively. The dependence of the dielectric constant on the applied magnetic field is a novel magnetoelectric effect. For $\mathbf{b}||\mathbf{e}$ the contribution $\delta\epsilon_D$ is positive and can be very large, while for $\mathbf{b}\perp\mathbf{e}$ the contribution $\delta\epsilon_D$ is negative. The expressions for arbitrary angle between \mathbf{b} and \mathbf{e} , and the relation to the angle between applied fields \mathbf{B} and \mathbf{E} , which is generally different due to properties of the anisotropy transformation, are given in Sec. S7 of [34].

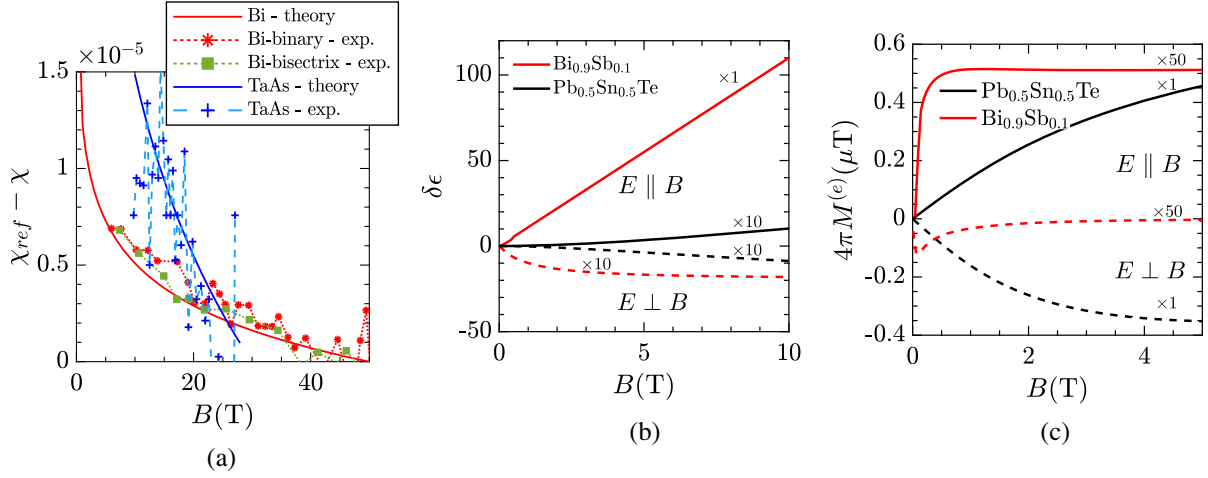


FIG. 2. (a) Nonlinear diamagnetic susceptibility $\chi_{\text{ref}} - \chi$ versus magnetic field, $\chi_{\text{ref}} = \chi(50 \text{ T})$ in Bi and $\chi_{\text{ref}} = \chi(30 \text{ T})$ in TaAs. In TaAs (blue) the field is along the crystal c direction and in Bi there are two directions, binary (red) and bisectrix (green). The points represent numerical differentiation of TaAs and Bi magnetization data from Refs. [31,32], respectively. The experimental points are connected by dashed lines for guidance. Solid lines represent our theory. The red solid line is our prediction for $\text{Bi}_{0.9}\text{Sb}_{0.1}$. (b) Predicted variation of the dielectric constant in magnetic field, for parallel (perpendicular) field configurations shown by solid (dashed) lines. (c) Predicted electric field modulated magnetization as a function of applied magnetic field, along the magnetic field direction at $E = 0.3E_*$.

Furthermore, according to (1) and (10), there is a nonlinear contribution quadratic in the electric field,

$$\delta\epsilon_D(\mathbf{E}) = \mathcal{U}^2 \frac{2\alpha_D}{15\pi} |\mathbf{e}|^2, \quad |\mathbf{b}| = 0, \quad (14)$$

which is suppressed by $|\mathbf{e}|^2/|\mathbf{b}|$ when $|\mathbf{b}| \gg 1$. Notably, at $|\mathbf{e}|, |\mathbf{b}| \ll 1$, contributions (13) and (14) add up.

The magnetic field induced variation of the dielectric constant in Eq. (13) scales as $\delta\epsilon_D \propto 1/B_* \propto \Delta^{-2}$. Thus, the effect is most significant in small band gap Dirac insulators. In Fig. 2(b), we plot our predictions for $\text{Bi}_{0.9}\text{Sb}_{0.1}$. For $\mathbf{e} \parallel \mathbf{b}$ the effect is enormous, $\delta\epsilon_D \sim 10/\text{T}$. For $\mathbf{E} \perp \mathbf{B}$ the effect is smaller and has the negative sign. In the same Fig. 2(b), we also plot predictions for $\delta\epsilon_D$ in $\text{Pb}_{0.5}\text{Sn}_{0.5}\text{Te}$. This compound has a larger gap, and therefore the effect is smaller, but still observable.

One more novel magnetoelectric effect is the dependence of magnetization on the applied electric field. The electric field-dependent magnetization $\mathbf{M}^{(e)} = (\partial\delta L/\partial\mathbf{B})$, in units of Dirac magnetons per ‘‘Dirac volume,’’ reads

$$4\pi\mathbf{M}^{(e)} = \frac{\mathcal{U}^{-1}\mathbf{b}}{|\mathbf{b}|} \frac{\mu_D}{3\pi\lambda_D^3} |\mathbf{e}|^2 D_i(|\mathbf{b}|),$$

$$|\mathbf{b}| \ll 1: D_{\parallel}(|\mathbf{b}|) = \frac{2}{3}|\mathbf{b}|, \quad D_{\perp}(|\mathbf{b}|) = -\frac{4}{15}|\mathbf{b}|,$$

$$|\mathbf{b}| \gg 1: D_{\parallel}(|\mathbf{b}|) = 1, \quad D_{\perp}(|\mathbf{b}|) = -\frac{1}{|\mathbf{b}|}. \quad (15)$$

The direction of the magnetization (15) in a Dirac crystal is defined by the vector \mathbf{b} and depends on crystal anisotropy as described by Eq. (3). Dimensionless functions $D_i(|\mathbf{b}|)$ in

the whole range of \mathbf{b} obtained by numerical integration of (9) are plotted in Fig. S2 in the Supplemental Material [34]. For $\mathbf{b} \parallel \mathbf{e}$ the magnetization is large and paramagnetic, while for $\mathbf{b} \perp \mathbf{e}$ the magnetization is diamagnetic [82]. Magnetization (15) is quadratic in the applied electric field and, as a function of magnetic field, saturates when $|\mathbf{b}| \gg 1$.

To enhance the magnetization in Eq. (15) one needs the electric field as strong as possible. However, the field is limited by the dielectric strength, E_d of the material, beyond which dielectric breakdown occurs. The breakdown probability (rate of Zener tunneling by electric field per unit volume) is obtained from Eq. (9) [25] and found to be $P \propto |\mathbf{e}|^2 e^{-\pi/|\mathbf{e}|}$ (See Sec. S4 in [34]). The most important aspect here is the exponential dependence, which universally applies to both the Dirac spectrum and quadratic dispersion. Thus, one expects that E_d is proportional to E_* . Taking two band insulators, diamond ($2\Delta \approx 5.5 \text{ eV}$, $E_d \approx 10^7 \text{ V/cm}$) and silicon ($2\Delta \approx 1.14 \text{ eV}$, $E_d \approx 3 \times 10^5 \text{ V/cm}$), as reference materials, we observe that the dielectric strength scales as $E_d \propto \Delta^2$. Therefore, E_d is a fixed fraction of E_* . Significant E -dependent magnetic effects [Eq. (15)] can then be observed for $|\mathbf{e}| = 0.1\text{--}0.3$ [83]. Furthermore, as usual in solids, setups with huge built-in electric fields in the insulating regime can be explored [84].

For a fixed $\mathbf{e} = E/E_*$, the electric field modulated magnetization in Eq. (15) obeys $M^{(e)} \propto B_* \propto \Delta^2$, so materials with a large gap are preferable, unlike in the dependence of the dielectric constant on magnetic field. In Fig. 2(c), we plot the predicted magnetization for $\text{Pb}_{0.5}\text{Sn}_{0.5}\text{Te}$ versus magnetic field at $E = 10^4 \text{ V/cm}$,

which corresponds to $\mathbf{e} \approx 0.3$. For both fields \mathbf{e} and \mathbf{b} , parallel to the c axis, the electric field driven magnetization is $4\pi M^{(e)} \approx 0.2 \mu\text{T}$ at $B = 1$ T. When $\mathbf{E} \perp \mathbf{B}$, the magnetization changes sign, see Fig. 2(c). In the same figure, we also plot the magnetization in $\text{Bi}_{0.9}\text{Sb}_{0.1}$ for $\mathbf{e} \approx 0.3$. Here the effect is smaller due to the smaller Dirac gap.

The electric field driven magnetization in $\text{Bi}_{0.9}\text{Sb}_{0.1}$ ($4\pi M^{(e)} \sim 10^{-8}$ T) and in $\text{Pb}_{0.5}\text{Sn}_{0.5}\text{Te}$ ($4\pi M^{(e)} \sim 2 \times 10^{-7}$ T) can be feasibly detected in lock-in experiments in an applied electric field having a constant and an ac component (with frequency ω). The induced magnetization is then characterized by contributions modulated at frequencies ω and 2ω . Of course, the condition $\hbar\omega \ll 2\Delta$ is assumed fulfilled. Experiments on observation of $M^{(e)}$ could also take advantage of the SQUID magnetometry, sensitive to magnetization as low as 10^{-15} T/ $\sqrt{\text{Hz}}$ [85], much lower than the predicted values.

In conclusion, based on the Heisenberg-Euler theory of the physical vacuum, we develop the theory of nonlinear electromagnetic effects in Dirac materials. We explain the results of two recent experiments on nonlinear contribution to magnetization of Dirac materials. We predict two novel magnetoelectric effects and discuss possible experiments and materials for their observation.

We thank M. O'Brien, H. Takagi, A. O. Sushkov, V. M. Shabaev, J. Seidel, A. R. Hamilton, U. Zuelicke, and Y. Ashim for useful comments. Y. L. G. was supported by the U.S. Department of Energy, Office of Basic Energy Sciences, Division of Materials Sciences and Engineering under Award No. DE-SC0010544. Y. L. G. also acknowledges the Gordon Godfrey bequest for the support of his visit to UNSW. A. C. K. and O. S. acknowledge the support from the Australian Research Council Centre of Excellence in Future Low Energy Electronics Technologies (CE170100039).

[1] W. Heisenberg and H. Euler, *Z. Phys.* **98**, 714 (1936).

[2] J. Schwinger, *Phys. Rev.* **82**, 664 (1951).

[3] V. M. Kaspi and A. M. Beloborodov, *Annu. Rev. Astron. Astrophys.* **55**, 261 (2017); A. Reisenegger, arXiv:astro-ph/0103010.

[4] K. Tuchin, *Adv. High Energy Phys.* **2013**, 490495 (2013).

[5] M. Marklund and P. K. Shukla, *Rev. Mod. Phys.* **78**, 591 (2006).

[6] S. Z. Akhmedaliev, G. Y. Kezerashvili, S. G. Klimenko, V. M. Malyshev, A. L. Maslennikov, A. M. Milov, A. I. Milstein, N. Y. Muchnoi, A. I. Naumenkov, V. S. Panin, S. V. Peleganchuk, V. G. Popov, G. E. Pospelov, I. Y. Protopopov, L. V. Romanov, A. G. Shamov, D. N. Shatilov, E. A. Simonov, and Y. A. Tikhonov, *Phys. Rev. C* **58**, 2844 (1998).

[7] L. Fedeli, A. Sainte-Marie, N. Zaim, M. Thévenet, J. L. Vay, A. Myers, F. Quéré, and H. Vincenti, *Phys. Rev. Lett.* **127**, 114801 (2021).

[8] M. H. Cohen and E. I. Blount, *Philos. Mag. A* **5**, 115 (1960).

[9] B. Lax, J. G. Mavroides, H. J. Zeiger, and R. J. Keyes, *Phys. Rev. Lett.* **5**, 241 (1960).

[10] P. Wolff, *J. Phys. Chem. Solids* **25**, 1057 (1964).

[11] X.-L. Qi, T. L. Hughes, and S.-C. Zhang, *Phys. Rev. B* **78**, 195424 (2008).

[12] H. Zhang, C.-X. Liu, X.-L. Qi, X. Dai, Z. Fang, and S.-C. Zhang, *Nat. Phys.* **5**, 438 (2009).

[13] M. Z. Hasan and C. L. Kane, *Rev. Mod. Phys.* **82**, 3045 (2010).

[14] Y. Ando, *J. Phys. Soc. Jpn.* **82**, 102001 (2013).

[15] T. Wehling, A. Black-Schaffer, and A. Balatsky, *Adv. Phys.* **63**, 1 (2014).

[16] D. Culcer, A. C. Keser, Y. Li, and G. Tkachov, *2D Mater.* **7**, 022007 (2020).

[17] I. Sodemann and L. Fu, *Phys. Rev. Lett.* **115**, 216806 (2015).

[18] O. Matsyshyn and I. Sodemann, *Phys. Rev. Lett.* **123**, 246602 (2019).

[19] H. Rostami and E. Cappelluti, *npj 2D Mater. Appl.* **5**, 50 (2021).

[20] H. Rostami and E. Cappelluti, *Phys. Rev. B* **103**, 125415 (2021).

[21] P. Bhalla, A. H. MacDonald, and D. Culcer, *Phys. Rev. Lett.* **124**, 087402 (2020).

[22] Z. Z. Du, C. M. Wang, H.-P. Sun, H.-Z. Lu, and X. C. Xie, *Nat. Commun.* **12**, 5038 (2021).

[23] T. Morimoto and N. Nagaosa, *Phys. Rev. B* **93**, 125125 (2016).

[24] A. Akhiezer and V. Berestetskii, *Quantum Electrodynamics*, Interscience Monographs and Texts in Physics and Astronomy Vol. XI (Interscience Publishers, New York, 1965).

[25] V. Berestetskii, E. Lifshitz, and L. Pitaevskii, *Quantum Electrodynamics: Volume 4*, Course of theoretical physics (Elsevier Science, New York, 1982).

[26] M. Peskin and D. Schroeder, *An Introduction to Quantum Field Theory*, Advanced book program (CRC Press, Boca Raton, 2018).

[27] G. V. Dunne, *From Fields to Strings: Circumnavigating Theoretical Physics* (World Scientific, Singapore, 2005), pp. 445–522.

[28] The high-order nonlinear electromagnetic effects can also emerge in two-dimensional materials [29], but is unrelated to the effects we discuss here, due to dimensionality considerations. For applications to $\text{SU}(N)$ gauge fields, see Ref. [30].

[29] M. Katsnelson, G. Volovik, and M. Zubkov, *Ann. Phys. (Amsterdam)* **331**, 160 (2013).

[30] A. N. Redlich, *Phys. Rev. D* **29**, 2366 (1984).

[31] C.-L. Zhang, C. M. Wang, Z. Yuan, X. Xu, G. Wang, C.-C. Lee, L. Pi, C. Xi, H. Lin, N. Harrison, H.-Z. Lu, J. Zhang, and S. Jia, *Nat. Commun.* **10**, 1028 (2019).

[32] A. Iwasa, A. Kondo, S. Kawachi, K. Akiba, Y. Nakanishi, M. Yoshizawa, M. Tokunaga, and K. Kindo, *Sci. Rep.* **9**, 1672 (2019).

[33] In Gaussian units. In an anisotropic material ϵ and μ are symmetric 3×3 matrices. Some QED textbooks are opposite to the condensed matter convention, see the footnote in

- Sec. 129 of Ref. [25]. In this Letter, $\mathbf{B} = \mu\mathbf{H}$ is the magnetic flux density and $\mathbf{E} = \epsilon^{-1}\mathbf{D}$ is the screened electric field.
- [34] See Supplemental Material at <http://link.aps.org/supplemental/10.1103/PhysRevLett.128.066402> for details of the derivation of anisotropic one-loop effective action, the calculation of nonlinear susceptibilities, a detailed comparison of our theory in different materials, and QED, which includes Refs. [35–63].
- [35] A. Abrikosov, *Fundamentals of the Theory of Metals* (Dover Publications, New York, 2017).
- [36] E. E. Salpeter and H. A. Bethe, *Phys. Rev.* **84**, 1232 (1951).
- [37] N. Birrell, N. Birrell, and P. Davies, *Quantum Fields in Curved Space*, Cambridge Monographs on Mathematical Physics (Cambridge University Press, Cambridge, England, 1984).
- [38] E. Burstein, S. Perkowitz, and M. Brodsky, *J. Phys. (Paris), Colloq.* **29**, C4 (1968).
- [39] F. J. Dyson, *Phys. Rev.* **85**, 631 (1952).
- [40] J. Fröhlich, *Rev. Math. Phys.* **30**, 1840007 (2018).
- [41] M. Gell-Mann and K. A. Brueckner, *Phys. Rev.* **106**, 364 (1957).
- [42] G. Giuliani and G. Vignale, *Quantum Theory of the Electron Liquid*, Masters Series in Physics and Astronomy (Cambridge University Press, Cambridge, England, 2005).
- [43] F. Herman, R. L. Kortum, I. B. Ortenburger, and J. P. Van Dyke, *J. Phys. (Paris), Colloq.* **29**, C4-62 (1968).
- [44] H. Hayasaka and Y. Fuseya, *J. Phys. Condens. Matter* **28**, 31LT01 (2016).
- [45] P. Schwerdtfeger and J. K. Nagle, *Mol. Phys.* **117**, 1200 (2019).
- [46] A. Jain, S. P. Ong, G. Hautier, W. Chen, W. D. Richards, S. Dacek, S. Cholia, D. Gunter, D. Skinner, G. Ceder, and K. a. Persson, *APL Mater.* **1**, 011002 (2013).
- [47] Y. Kanai and K. Shohno, *Jpn. J. Appl. Phys.* **2**, 6 (1963).
- [48] B. A. Lippmann and J. Schwinger, *Phys. Rev.* **79**, 469 (1950).
- [49] L. D. Landau, *Collected Papers of L.D. Landau*, edited by D. Ter Haar (Pergamon, 1965), pp. 607–610, [10.1016/B978-0-08-010586-4.50083-3](https://doi.org/10.1016/B978-0-08-010586-4.50083-3).
- [50] P. J. Lin and L. Kleinman, *Phys. Rev.* **142**, 478 (1966).
- [51] I. Lefebvre, M. Lannoo, G. Allan, A. Ibanez, J. Fourcade, J. C. Jumas, and E. Beaurepaire, *Phys. Rev. Lett.* **59**, 2471 (1987).
- [52] N. F. Mott, *Proc. R. Soc. A* **167**, 384 (1938).
- [53] I. Huet, M. R. De Trautenberg, and C. Schubert, *Int. J. Mod. Phys.* **14**, 383 (2012).
- [54] R. Rudolph, H. Krüger, B. Fellmuth, and R. Herrmann, *Phys. Status Solidi (b)* **102**, 295 (1980).
- [55] I. M. Suslov, *J. Exp. Theor. Phys.* **108**, 980 (2009).
- [56] E. Schrödinger, *Ann. Phys. (Berlin)* **384**, 361 (1926).
- [57] A. Svane, N. E. Christensen, M. Cardona, A. N. Chantis, M. van Schilfgaarde, and T. Kotani, *Phys. Rev. B* **81**, 245120 (2010).
- [58] N. Suzuki and S. Adachi, *Jpn. J. Appl. Phys.* **34**, 5977 (1995).
- [59] Antimony telluride (Sb_2Te_3) dielectric constants, in *Non-Tetrahedrally Bonded Elements and Binary Compounds I*, edited by O. Madelung, U. Rössler, and M. Schulz, Landolt-Börnstein, Group III Condensed Matter, Vol. 41c (Springer-Verlag, Berlin, Heidelberg, 1998), [10.1007/10681727_1045](https://doi.org/10.1007/10681727_1045).
- [60] Bismuth telluride (Bi_2Te_3) dielectric constants, in *Non-Tetrahedrally Bonded Elements and Binary Compounds I*, edited by O. Madelung, U. Rössler, and M. Schulz, Landolt-Börnstein, Group III Condensed Matter, Vol. 41c (Springer-Verlag, Berlin, Heidelberg, 1998), [10.1007/10681727_963](https://doi.org/10.1007/10681727_963).
- [61] Bismuth selenide (Bi_2Se_3) dielectric constants, in *Non-Tetrahedrally Bonded Elements and Binary Compounds I*, edited by O. Madelung, U. Rössler, and M. Schulz, Landolt-Börnstein, Group III Condensed Matter, Vol. 41c (Springer-Verlag, Berlin, Heidelberg, 1998), [10.1007/10681727_945](https://doi.org/10.1007/10681727_945).
- [62] H. Weng, C. Fang, Z. Fang, B. A. Bernevig, and X. Dai, *Phys. Rev. X* **5**, 011029 (2015).
- [63] G. H. Wannier, *Phys. Rev.* **52**, 191 (1937).
- [64] A. G. Aronov and G. E. Pikus, *Sov. Phys. JETP* **24**, 188 (1967) [*J. Exp. Theor. Phys.* **51**, 281 (1966)].
- [65] When the band gap is inverted, as in topological insulators, our analysis applies to $|\Delta|$. The additional boundary term in the effective action of the electromagnetic field, proportional to $\mathbf{E} \cdot \mathbf{B}$ in topological insulators [40] and Weyl semimetals [66–68] does not affect the nonlinear response that we investigate in this letter.
- [66] A. Burkov, *Annu. Rev. Condens. Matter Phys.* **9**, 359 (2018).
- [67] Z. M. Raines and V. M. Galitski, *Phys. Rev. B* **96**, 161115 (R) (2017).
- [68] C. Rylands, A. Parhizkar, A. A. Burkov, and V. Galitski, *Phys. Rev. Lett.* **126**, 185303 (2021).
- [69] J. J. Thomson, *Philos. Mag.* **44**, 293 (1897); R. A. Millikan, *Phys. Rev.* **2**, 109 (1913).
- [70] E. Tiesinga, P. J. Mohr, D. B. Newell, and B. N. Taylor, *J. Phys. Chem. Ref. Data* **50**, 033105 (2021).
- [71] P. Dziawa, B. J. Kowalski, K. Dybko, R. Buczko, A. Szczerbakow, M. Szot, E. Łusakowska, T. Balasubramanian, B. M. Wojek, M. H. Berntsen, O. Tjernberg, and T. Story, *Nat. Mater.* **11**, 1023 (2012).
- [72] Y. Liu and R. E. Allen, *Phys. Rev. B* **52**, 1566 (1995).
- [73] D. Hsieh, D. Qian, L. Wray, Y. Xia, Y. S. Hor, R. J. Cava, and M. Z. Hasan, *Nature (London)* **452**, 970 (2008).
- [74] L. Fu and C. L. Kane, *Phys. Rev. B* **76**, 045302 (2007); A. Bansil, H. Lin, and T. Das, *Rev. Mod. Phys.* **88**, 021004 (2016).
- [75] TaAs is noncentrosymmetric crystal, but since it is gapless, we take $E = 0$ to avoid transport. TaAs is nonmagnetic and the time reversal symmetry requires that the effective action contains even powers of B only.
- [76] L. J. Sham, *Phys. Rev.* **150**, 720 (1966).
- [77] L. J. Sham and T. M. Rice, *Phys. Rev.* **144**, 708 (1966).
- [78] Y. Fuseya, M. Ogata, and H. Fukuyama, *J. Phys. Soc. Jpn.* **84**, 012001 (2015).
- [79] $|\mathbf{e}|, |\mathbf{b}| \ll \Lambda^2/\Delta^2$, otherwise the effective Dirac Hamiltonian no longer applies. See Sec. S5 in [34].
- [80] The exact result is obtained by directly summing the energies of Landau levels [24,25] or, in modern language, zeta-function regularization [27].
- [81] However, our approach from the vantage point afforded by the transformation of Heisenberg-Euler action under dila-

tion and contraction of space (see Sec. S1 in [34]) leads to a more accurate overall factor.

- [82] The angle between \mathbf{e} and \mathbf{b} , in general, is different than the one between applied fields \mathbf{B} and \mathbf{E} . The transformation of the angle is given in Sec. S1 [34]. The susceptibilities for arbitrary angle between \mathbf{b} and \mathbf{e} are given in Secs. S6 and S7 [34].
- [83] Of course, there are other factors, like the dependence of dielectric strength on impurities, the size of the sample, etc.
- [84] A. R. Calawa, R. H. Rediker, B. Lax, and A. L. McWhorter, *Phys. Rev. Lett.* **5**, 55 (1960); R. H. Rediker and A. R. Calawa, *J. Appl. Phys.* **32**, 2189 (1961).
- [85] A. V. Gramolin, D. Aybas, D. Johnson, J. Adam, and A. O. Sushkov, *Nat. Phys.* **17**, 79 (2021).